Journal of Controlled Release 328 (2020) 87–99

Contents lists available at ScienceDirect

Journal of Controlled Release

journal homepage: www.elsevier.com/locate/jconrel

Tumor microenvironment-responsive and oxygen self-sufficient oil droplet nanoparticles for enhanced photothermal/photodynamic combination therapy against hypoxic tumors☆

Reesha Kv[a,1], Te-I Liu[a,1], I.-Lin Lu[a,b], Chia-Chen Liu[a], Hsin-Hung Chen[a], Ting-Yu Lu[a], Wen-Hsuan Chiang[c,*], Hsin-Cheng Chiu[a,*]

[a] Department of Biomedical Engineering and Environmental Sciences, National Tsing Hua University, Hsinchu 30013, Taiwan
[b] Department of Surgery, Hsinchu Mackay Memorial Hospital, Hsinchu City 30071, Taiwan
[c] Department of Chemical Engineering, National Chung Hsing University, Taichung 402, Taiwan.

ARTICLE INFO

Keywords:
Self-sufficient oxygen delivery
Photothermal/photodynamic combination therapy
Tumor acidity responsive
Tumor hypoxia
Lipid-enclosed droplets

ABSTRACT

The combination of photothermal and photodynamic therapy (PTT/PDT) shows pronounced potential as a prominent therapeutic strategy for tumor treatment. However, the efficacy is limited by insufficient tumor-targeted delivery of PTT and PDT reagents and the hypoxic nature of the tumor microenvironment. To overcome these limitations, tumor acidity-responsive lipid membrane-enclosed perfluorooctyl bromide oil droplet nanoparticles (NPs) surface modified with *N*-acetyl histidine-modified D-α-tocopheryl polyethylene glycol 1000 succinate (PFOB@IMHNPs) were developed, capable of co-delivering oxygen, IR780 (a photothermal agent) and mTHPC (a photodynamic sensitizer) into tumors. Through self-sufficient oxygen transportation in combination with promotion of cellular uptake upon acid-triggered generation of surface positive charge, the PFOB@IMHNPs effectively delivered IR780 and mTHPC and produced singlet oxygen within hypoxic TRAMP-C1 cells following exposure to irradiation at 660 nm. This led to effective killing of hypoxic cancer cells *in vitro*. Importantly, when irradiation at 808 and 660 nm was carried out, PT/PD combination therapy utilizing PFOB@IMHNPs dramatically suppressed the growth of TRAMP-C1 tumors through effective tumor-targeted cargo delivery and relief of tumor hypoxia. Our results suggest the high potential of the PFOB@IMHNPs developed in this study in clinical application for cancer treatment.

1. Introduction

In the past decade, phototherapeutic approaches such as the well-known techniques of photothermal therapy (PTT) and photodynamic therapy (PDT) have attracted considerable attention for their applications in solid tumor treatment due to their minimally invasive nature, high spatial–temporal selectivity and low systemic toxicity in comparison with traditional chemotherapy and radiotherapy [1–6]. There have been a number of studies investigating the benefits of combined PTT and PDT for the treatment of tumors [5–9]. Under appropriate photo-irradiation, the reagents used in PTT convert light energy into heat, resulting in localized tumor ablation [5,10]. However, inadequate tumor-targeted delivery of PTT reagents can lead to insufficient tumor hyperthermia, with a concomitant reduction in efficacy with potential tumor recurrence [5,11]. In contrast, the use of photosensitizers in PDT can produce toxic reactive oxygen species (ROS) when exposed to specific photo-irradiation with an adequate oxygen (O_2) source, resulting in the killing of cancer cells [12–14]. Unfortunately, the tumor cells in hypoxic regions (below 2% O_2) are highly resistant to PDT, which lowers the antitumor effects of this treatment [15–17].

In order to improve the therapeutic outcomes of combined PTT and PDT, it is clear that selective accumulation of PTT and PDT reagents within tumor sites together with self-sufficient tumor-targeted oxygen delivery is highly desired. To this end, several new strategies have been recently proposed to reduce tumor hypoxia [5,7,9,15–17]; for example, mitochondria-targeted perfluorooctyl bromide (PFOB)-containing nanoliposomes as carriers of IR780, a PDT/PTT reagent, and oxygen have been developed for use with amplified synergistic cancer phototherapy

☆ This paper is dedicated to Professor Jindrich Kopecek on the occasion of his 80th birthday.

* Corresponding authors.
E-mail addresses: whchiang@dragon.nchu.edu.tw (W.-H. Chiang), hscchiu@mx.nthu.edu.tw (H.-C. Chiu).

[1] These authors contributed equally to this work.

https://doi.org/10.1016/j.jconrel.2020.08.038
Received 20 May 2020; Received in revised form 28 July 2020; Accepted 20 August 2020
Available online 26 August 2020

[5]. PFOB was employed to serve as an oxygen depot taking advantages of its superior capability of oxygen dissolution. Under guidance by computed tomography and photoacoustic and fluorescence imaging, irradiation with near infrared (NIR) at 808 nm that activated these IR780-carrying nanoliposomes, termed "Nano-RBCs," has been shown to completely eradicated tumors through self-sufficient oxygen-enhanced PDT due to their mitochondria-targeting functions in synergistic PDT/PTT, with no apparent recurrence observed. Du et al. adopted a layer-by-layer approach to construct multifunctional photo-responsive NPs consisting of a heat-generating gold nanostar core coated with layers of oxygen-generating manganese dioxide, chlorin e6 and hyaluronic acid (which targets CD44) in sequence [7]. *In vitro* cell studies have demonstrated these NPs to be significantly uptaken by CD44-overexpressing MDA-MB-231 cells, with efficient production of oxygen under acidic, H_2O_2-rich conditions. When exposed to irradiation by 808- and 650-nm NIR lasers, these NPs effectively kill cancer cells through PTT and PDT combination therapy. It has also been reported that coating Prussian blue (PB) NPs with zirconium-porphyrin (PCN) shells resulted in the generation of core-shell nanohybrids (PB@PCN) and further coating with a homologous tumor cell membrane produced particles (PB@PCN@MEM) with good immune evasion and active tumor-targeting abilities [9]. The nanohybrid particles are designed as a tandem catalyst capable of transforming endogenous H_2O_2 to O_2 directly released into the PCN framework, thus reducing tumor hypoxia and boosting the antitumor potency of PDT. Furthermore, the expression of heat-shock proteins, which are upregulated after PTT, was reduced through the use of these particles. The homotypic targeting and immune-evading capacity of the PB@PCN@MEM particles led to sufficient deposition in CT-26 tumors, with remarkable inhibition of tumor growth observed following image-guided combined PTT/PDT therapy.

In addition to the effects of oxygen delivery on tumor hypoxia, the properties of NP-based delivery that enhance tumor accumulation and cellular uptake of PTT/PDT agents are also crucial to improving antitumor effects of these therapies. Furthermore, the extracellular acidity of solid tumors (pH_e 6.5–7.0) has been exploited to enhance the cellular uptake of therapeutic nanoformulations within solid tumors through the design of various smart NP-based therapeutic delivery systems capable of changing their PEGylation [18,19], size [20,21], surface charge [22–24], or targeting [25,26] in response to acidic conditions. In our previous work [10], we have reported the synthesis of pH_e-sensitive *N*-acetyl histidine-modified D-α-tocopheryl polyethylene glycol 1000 succinate (NAcHis-TPGS) and subsequent coating onto the surfaces of poly(lactic-co-glycolic acid)-based cores loaded with indocyanine green and doxorubicin. The resulting payload-carrying NPs enabled significant deposition within murine TRAMP-C1 prostate solid tumors and actively infiltrated into deep-tumor hypoxic environment due to their pH_e-triggered near-neutral surfaces and additional hitchhiking transport *via* tumor-associated microphages. Tumor growth was highly suppressed by adopting these functionalized NP therapeutics for imaging-guided combined PTT and chemotherapy.

The present article describes the fabrication of pH_e-responsive therapeutic NPs based upon phospholipid membrane-enclosed PFOB droplets obtained from co-assembly of PFOB, dipalmitoylphosphatidylcholine (DPPC), cholesterol, and NAcHis-TPGS to co-deliver oxygen, IR780 (a PTT agent) and meta-tetra(hydroxyphenyl)chlorin (mTHPC) (a PDT agent) into the tumor with the aim of augmenting the antitumor efficacy of PT/PD combination therapy (Scheme 1). Taking advantages of the increased surface positive charge due to acid-activated protonation of NAcHis moieties in combination with self-sufficient oxygen delivery, the tailor-made oil droplet NPs (*i.e.*, IR780/mTHPC-loaded, NAcHis-TPGS modified lipid membrane- enclosed PFOB droplet NPs (PFOB@IMHNPs)) considerably promoted the intracellular delivery of IR780 and mTHPC under acidic conditions and increased intracellular generation of ROS in hypoxic environments upon NIR irradiation, leading to efficient killing of TRAMP-C1 cells. The pronounced effects of PFOB@IMHNPs on enhanced accumulation of PTT/PDT agents within TRAMP-C1 tumors, effective tumor-targeted cargo delivery, relief of tumor hypoxia and potent suppression of tumor growth upon NIR laser irradiation were demonstrated, showing great promise of PFOB@IMHNPs for cancer therapy.

2. Materials and methods

2.1. Materials

NAcHis-TPGS used in this study was synthesized and characterized according to our previous report [10]. DPPC was purchased from Avanti Polar Lipids, Inc. (USA), and PFOB, cholesterol, IR780, mTHPC, 2′,7'dichlorodihydrofluorescein diacetate acid (DCFH-DA), 3-(4,5-dimethylthiazol-2-yl)-2,5-diphenyltetrazolium bromide (MTT), and pimonidazole (PIMO) were supplied by Sigma-Aldrich (USA). Singlet oxygen sensor green (SOSG) reagent was obtained from Molecular Probes Inc. (USA). Deionized water was produced in-house using a Milli-Q Synthesis system (18 MΩ, Millipore). All other chemicals were of reagent grade and were used as received. For cell culture studies, Dulbecco's modified Eagle's medium (DMEM), fetal bovine serum (FBS), 0.25% trypsin-ethylenediaminetetraacetic acid (EDTA) solution, penicillin–streptomycin solution, and Hoechst 33342 were purchased from Thermo Fisher Scientific (Waltham, MA, USA). Anti-hypoxia-inducible factor 1 alpha (HIF-1α)-fluorescein was obtained from Invitrogen (USA). TRAMP-C1 cells (a murine prostate cancer cell line) were obtained from the Food Industry Research and Development Institute (Hsinchu City, Taiwan). Male C57BL/6 mice (4–5 weeks old) were purchased from the National Laboratory Animal Center, Taiwan. Approved guidelines for the care and use of laboratory animals from the Institutional Animal Care and Use Committee (approved number for animal use; IACUC 10466) were followed throughout the study.

2.2. NP preparation

Various cargo-carrying lipid membrane-enclosed PFOB droplet NPs coated with either NAcHis-TPGS or pristine TPGS were prepared *via* thin-film hydration. PFOB@IMHNPs were prepared as follows: DPPC (4.0 mg), cholesterol (1.0 mg), NAcHis-TPGS (1.0 mg), IR780 (0.6 mg), and mTHPC (0.6 mg) were dissolved in chloroform (2.0 mL) and subjected to rotary evaporation to remove chloroform and create a thin film. The thin film was hydrated by addition of pH 7.4 phosphate buffer (10 mM, 0.95 mL) followed by ultrasonication in a water bath for 1 min. Next, PFOB (50 μL) was added into the solution and sonicated with a probe-type ultrasonicator (20 kHz, 750 W) operated at 20 °C for 20 min. The resulting solution was then centrifuged at 8000 rpm to remove unloaded IR780 and mTHPC species, and the purified PFOB@IMHNPs in pellets were collected. As control samples, dual drugs-loaded TPGS modified PFOB droplet NPs (PFOB@IMNPs) in the absence of the NAcHis moiety from the NP surfaces, drug-free NAcHis-TPGS modified PFOB droplet NPs (PFOB@HNPs), IR780/mTHPC/NAcHis-TPGS lipid-based NPs (IMHNPs), IR780/mTHPC/TPGS lipid-based NPs (IMNPs), and drug-free NAcHis-TPGS lipid-based NPs (HNPs) were prepared in a similar manner. For oxygen loading, PFOB-carrying NPs were purged with oxygen for 15 min, leading to the dissolution of oxygen in PFOB cores of the NPs. The PFOB-carrying NPs used in this study were all oxygenated. Oxygen loading of HNPs and IMHNPs as the controls was performed in a similar manner.

2.3. NP characterization

Particle size, size distribution, and zeta potential of different NPs in aqueous solutions were measured using dynamic light scattering (DLS) on a ZetaSizer Nano Series instrument (Malvern Instruments, UK). The data presented herein represent average values from at least triplicate measurements. The morphology of IMHNPs, PFOB@IMNPs, and PFOB@IMHNPs was evaluated by transmission electron microscopy

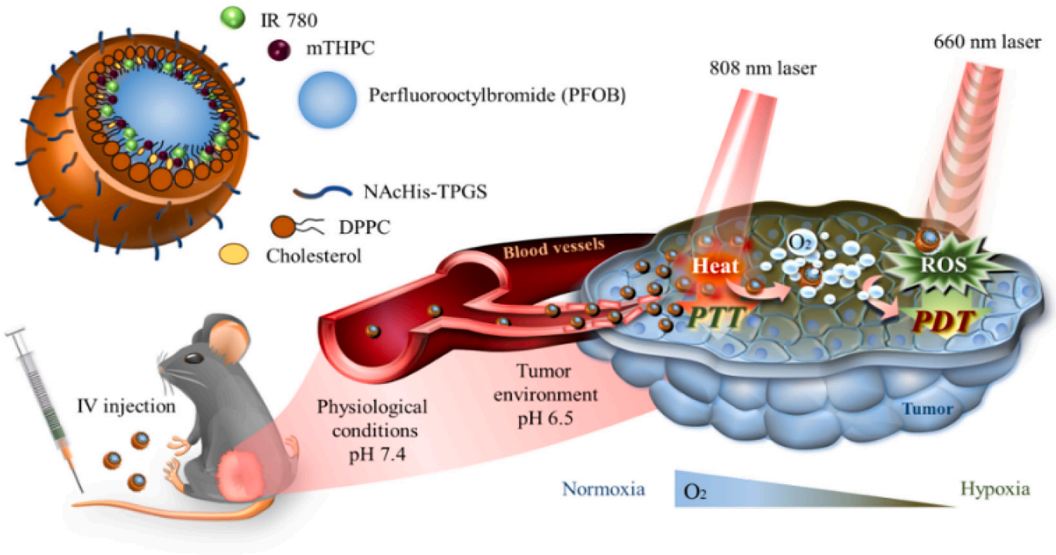

Scheme 1. Schematic illustration of the multiple functions of the tailor-made therapeutic NPs comprising PFOB droplets enclosed within a lipid membrane. NAcHis-TPGS introduced tumor acidity responsive charge transition whereas the lipid membrane-enclosed PFOB droplets conferred tumor-targeted oxygen delivery properties and enabled co-delivery of IR780 and mTHPC for improving the efficacy of photothermal/photodynamic combination therapy.

(TEM) (JEOL JEM-2100F, Japan). The absorption spectra of IR780/mTHPC-carrying NPs with or without PFOB encapsulation were acquired in phosphate buffered saline (PBS) using an ultraviolet/visible (UV/Vis) spectrophotometer (U2900, Hitachi, Japan).

To quantify the IR780 and mTHPC contents, a preset volume of cargo-containing NP solution was lyophilized and then dissolved in DMSO. The absorbances of IR780 and mTHPC at 780 and 660 nm, respectively, were determined. The drug-loading efficiency (DLE) and drug-loading content (DLC) were calculated using the following formulae:

$$\text{DLE}\ (\%) = (\text{weight of drug loaded/weight of drug in feed}) \times 100\%.$$

$$\text{DLC}\ (\%) = (\text{weight of drug loaded/total weight of cargo} - \text{loaded NPs}) \times 100\%.$$

To evaluate the aqueous photostability of IR780 encapsulated within various NPs, the UV/Vis absorption spectra of free IR780, PFOB@IMHNPs and PFOB@IHNPs in aqueous solutions were obtained after incubation at 37 °C for various time intervals using a UV/Vis spectrophotometer (U2900, Hitachi, Japan). Based on the UV/Vis absorption spectra, the maximum absorbance of IR780 at each preset time was normalized to that at the beginning.

To determine the temperature rise profiles, IR780-carrying NPs and free IR780 species in PBS (1.0 mL) were irradiated using an 808-nm NIR laser (power density, 1.0 W/cm^2) for 5 min. Solution temperatures were monitored with an infrared thermal imaging camera (Thermo Shot F20, NEC Avio Infrared Technologies, Germany) with the irradiation time. The oxygen-carrying capability of the PFOB droplet NPs and the effects of NIR-triggered hyperthermia on oxygen release were assessed by adding aqueous solutions (5.0 mL) of oxygenated NPs to degassed water (30.0 mL) and then measuring the oxygen concentration over time with a portable dissolved-oxygen meter (YSI, 550A, Japan). The oxygen concentration was also measured with the solution being subjected to irradiation using an 808-nm NIR laser for 10 min.

The NIR-activated singlet oxygen generation of oxygenated IMHNPs and PFOB@IMHNPs dispersed in either normal water (normoxia) or degassed water (hypoxia) was evaluated by SOSG assay. Briefly, particles with various mTHPC concentrations were dispersed in either normal or degassed water (2.0 mL) containing 10 μM SOSG and the aqueous solutions were irradiated with irradiation at 660 nm (5 min, 6 mW/cm^2) alone or 880 nm (5 min, 1.0 W/cm^2) plus 660 nm (5 min, 6 mW/cm^2). The fluorescence intensity of the solutions was measured at 530 nm with a fluorescence spectrometer (F-7000, Hitachi).

2.4. In vitro cellular uptake study

Free IR780/mTHPC, PFOB@IMHNPs, or PFOB@IMNPs were dispersed in DMEM at pH 7.4 or 6.5 to final IR780 and mTHPC concentrations of 10 and 9.7 μM, respectively. With TRAMP-C1 cells being seeded in 6-well culture plates at a density of 3×10^5 cells/well, the NP solutions were added and incubated at 37 °C for 4 h, after which the cells were washed three times with PBS. DMSO (0.65 mL) was then added to disrupt the cells and the fluorescence signals of IR780 (Ex. 710 nm and Em. 840 nm) was measured on an *In Vivo* Imaging System (IVIS; Xenogen IVIS Spectrum). The FACSCalibur flow cytometer (BD Bioscience) was used to evaluate cellular uptake of free IR780/mTHPC, PFOB@IMHNPs, and PFOB@IMNPs (9.7 μM mTHPC). After 4-h incubation, the treated TRAMP-C1 cells were detached with trypsin-EDTA solution and then re-suspended in PBS (1.0 mL). The mTHPC fluorescence of a minimum of 1×10^4 cells per batch was analyzed by plotting fluorescence intensity on a three-decade log scale. Cellular uptake was further explored by confocal laser scanning microscopy (CLSM) (ZEISS LSM-780, Germany). With TRAMP-C1 cells (3×10^5 cells/well) being seeded onto 22-mm round glass coverslips in 6-well plates and then incubated with free IR780/mTHPC, PFOB@IMHNPs, or PFOB@IMNPs (mTHPC concentration = 6.5 μg/mL) at pH 7.4 or 6.5 for 4 h. After being washed twice with PBS and immobilized with 4% formaldehyde, cells were stained with Hoechst 33342 to identify cell nuclei. Fluorescence images of cells were acquired at excitation wavelengths of 405 and 633 nm for Hoechst and mTHPC, respectively.

2.5. Intracellular ROS generation

The ROS generation in TRAMP-C1 cells incubated with IMHNPs or PFOB@IMHNPs and exposed to NIR irradiation under normoxic or hypoxic conditions was studied using DCFH-DA assay. TRAMP-C1 cells seeded on 22-mm round glass coverslips in 6-well plates at 3×10^5 cells/well were incubated with free IR780/mTHPC, IMHNPs, or PFOB@IMHNPs (at an IR780 concentration of 10 μM and mTHPC of 9.7 μM) at pH 7.4 or 6.5 for 4 h, followed by treatment with DCFH-DA (10 μM) for 30 min. Treated cells were then irradiated by either a single 660-nm NIR laser for 5 min or an 808-nm NIR laser combined with a 660-nm

NIR laser for 5 min (6 mW/cm^2). Thirty minutes after irradiation, treated cells were washed twice with PBS and immobilized with 4% formaldehyde. Cells were stained with Hoechst 33342 to visualize cell nuclei and fluorescence images were acquired at excitation wavelengths of 405 and 488 nm for Hoechst and DCF, respectively.

2.6. In vitro cytotoxicity examination

TRAMP-C1 cells were seeded in a 96-well plate at 8 × 10^3 cells/well in DMEM containing 10% FBS and 1% penicillin. Plates were incubated at 37 °C for 24 h in normoxic or hypoxic conditions. The medium was then replaced with fresh DMEM (100 μL) containing either PFOB@IMHNPs or IMHNPs with various concentrations of IR780 and the cells were further incubated for 4 h. After being rinsed with PBS twice, cells were dispersed in DMEM (200 μL) and exposed to irradiation at 808 nm (1.0 W/cm^2) for 5 min, followed by irradiation at 660 nm (6 mW/cm^2) for 5 min or irradiated at 660 nm (6 mW/cm^2) for 5 min alone. Irradiated cells were incubated for 18 h. MTT (0.25 mg/mL, 200 μL) was added into each well, and plates were incubated at 37 °C for 4 h. With the culture medium being removed, DMSO was added to dissolve the precipitate, and the absorbance of the DMSO solution at 570 nm was measured using a SpectraMax M5 microplate reader.

2.7. In vivo biodistribution and near-infrared-triggered tumor hyperthermia

To establish the animal tumor model, 6 × 10^7 TRAMP-C1 cells were subcutaneously injected into the left backs of male C57BL/6 mice. Tumor volume (V) was calculated as $V = L \times W^2/2$, where L and W are the tumor dimensions at the longest and shortest points, respectively. After tumor volume had increased to 200 mm^3, PBS, free IR780/mTHPC or various cargo-loaded NPs were injected into the mice *via* tail vein at an IR780 dosage of 2.5 mg/kg. The free IR780/mTHPC mixture used in this study as a control was obtained by a large dilution of the DMSO solution of IR780/mTHPC with PBS. At 24 h post-injection, mice were sacrificed and the tumor and major organs were harvested. *Ex vivo* imaging was carried out using the IVIS to evaluate the biodistribution of different nanoformulations. To assess *in vivo* NIR-activated tumor hyperthermia, at 24 h post-injection, the tumor site of mice treated with PBS, free IR780/mTHPC, or various cargo-loaded NPs was irradiated with an 808-nm laser (1.0 W/cm^2) for 5 min. The tumor local temperature was measured using an infrared thermal imaging camera.

2.8. Detection of tumor hypoxia status

Tumor hypoxia status was determined by HIF-1α and PIMO staining. After tumor volume had increased to 200 mm^3, the tumor-bearing mice were intravenously injected with PFOB@IMHNPs or IMHNPs. At 24 h post-injection, the mice were treated intraperitoneally with PIMO (10 mg/mL in PBS) 10 min before NIR laser irradiation at 808 nm (1.0 W/cm^2).The irradiation was carried out for 5 min. Mice were scarified and the tumors were harvested for cryo-sectioning. Rat anti-HIF-1α antibody, anti-PIMO antibody and Alexa Fluor 488® conjugated goat anti-rat secondary antibody were utilized for immunohistochemical (IHC) examination of tumor hypoxia in tumor tissue sections. The sections were also stained with Hoechst 33342 to identify cell nuclei. All stained tumor sections were examined on a CLSM equipped with fluorescence channels for Hoechst 33342, Alexa Fluor 488, FITC, and mTHPC.

2.9. In vivo antitumor effects

When the tumor volume reached 200 mm^3, mice were randomly divided into eight groups (six per group) and intravenously injected with PBS, free IR780/mTHPC, PFOB@IMHNPs, PFOB@IMNPs, or IMHNPs at an IR780 dosage of 2.5 mg/kg and an mTHPC dosage of 2.43 mg/kg. At 24 h post-injection, the tumor was irradiated for either 5 min with an 808-nm NIR laser (1.0 W/cm^2) plus 5 min with a 660-nm NIR laser (0.6 W/cm^2), 5 min at 660 nm (0.6 W/cm^2) alone, or 5 min at 808 nm (1.0 W/cm^2) alone. Tumor volumes and body weights were recorded daily for 14 days after irradiation. Mice were sacrificed at the end of the treatment, and the isolated tumors were weighed to calculate the therapeutic index (TI, defined as follows), which was adopted as a quantitative measure of therapeutic efficacy:

$$\mathrm{TI}\ (\%) = \left(1 - \frac{\text{Weight of tumor in the experimental group}}{\text{Weight of tumor in the control group}}\right) \times 100\%$$

2.10. Statistical analysis

All data are reported as mean ± standard deviation (SD). Student's *t*-test and one-way ANOVA were used to analyze the differences between the control and test groups. Statistical significance is indicated as (n.s.) $P > 0.05$, (*) $P < 0.05$, (**) $P < 0.01$ and (***) $P < 0.001$.

3. Results and discussion

3.1. Preparation and characterization of therapeutic oil droplet NPs

Various therapeutic NPs including the target sample, PFOB@IMHNPs, and other control samples, *i.e.*, PFOB@IMNPs, PFOB@HNPs, IMHNPs, IMNPs, and HNPs, were successfully prepared by the thin film hydration approach. Among them, PFOB@IMHNPs, PFOB@IMNPs, and PFOB@HNPs are membrane enclosed PFOB oil droplet NPs meanwhile the others are liposome-like NPs lacking PFOB to carry oxygen as control samples. As presented in Fig. 1a and Table 1, IMHNPs, IMNPs, and HNPs in aqueous solutions at pH 7.4 were comparable in terms of particle size and size distribution, indicating that neither drug encapsulation nor surface coating affected particle size. Notably, with PFOB oil droplets being enclosed with DPPC membranes, particle size was apparently enlarged as a result of the enhanced interfacial tension between oil droplets and surrounding aqueous phase. Moreover, PFOB@IMHNPs and PFOB@IMNPs appeared to be dark and spherical in shape and exhibited high contrast on TEM images compared with IMHNPs (Fig. 1b and S1). Successful incorporation of PFOB into NPs by enclosure with DPPC membranes leads to enhancement in TEM imaging due to the high electron density of the oil droplet, and similar TEM images of perfluorocarbon-containing NPs have been reported [27,28]. When the pH was adjusted from 7.4 to 6.0, the zeta potentials of PFOB@IMHNPs and IMHNPs change from *ca.* −10 mV to +5 mV (Fig. 1c), suggesting that acidity-triggered protonation of the imidazole groups of NAcHis-TPGS altered the particle surface charge to a significant extent. In contrast, the lack of pH-responsive NAcHis residue in TPGS meant that the zeta potentials of PFOB@IMNPs and IMNPs were virtually unchanged by pH reduction. It is noteworthy that, under mild acidic conditions (pH 6.5) which reflect the acidic tumor microenvironment, PFOB@IMHNPs exhibited approximately neutral zeta potential, suggesting the feasibility of enhancing uptake by cancer cells. When the medium pH was lowered from 7.4 to 6.0, no significant variation in particle size was observed for any cargo-loaded NPs (Fig. S2). No significant variation in particle size was observed for cargo-carrying NPs dispersed in DMEM or PBS over a period of 4 days (Fig. S3). This demonstrates that coating DPPC membrane-enclosed NPs with either TPGS or its NAcHis conjugate considerably enhances colloidal stability, most likely because the hydrophilic PEG chain segments increase steric repulsion and prevent interparticulate aggregation. Furthermore, it should be noted that the PFOB@IMHNPs and IMHNPs subjected to a large-volume dilution with PBS still maintained unvaried particle size (Fig. S4). Based on these findings, it was expected that the robust cargo-carrying NPs can preserve structural stability during blood circulation after intravenous administration to avoid inter-particle aggregation and colloidal disintegration.

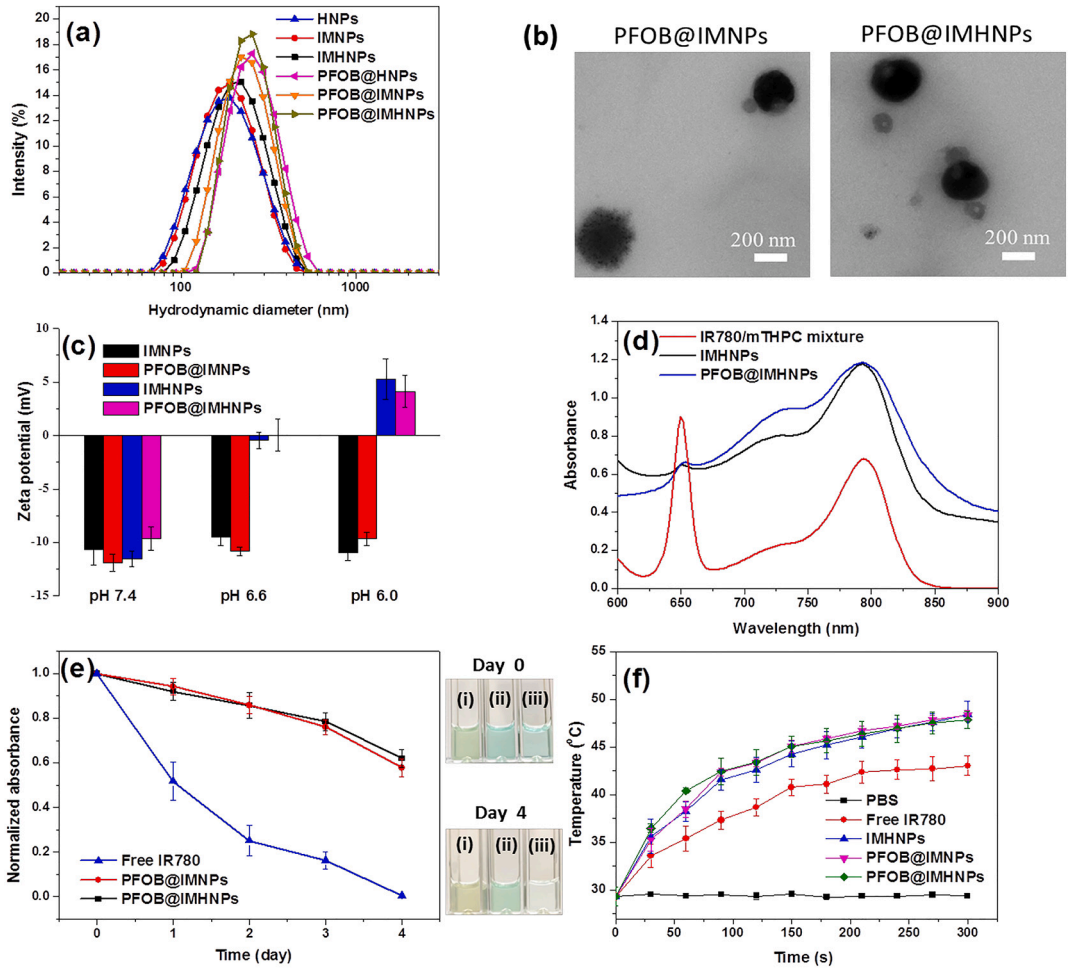

Fig. 1. (a) Size distribution profiles of various NPs in aqueous solution of pH 7.4 obtained by dynamic light scattering. (b) TEM images of PFOB@IMNPs and PFOB@IMHNPs. (c) Zeta potentials of various NPs in aqueous solutions of pH 6.0, 6.6 and 7.4. (d) Absorption spectra of IR780/mTHPC mixture in DMSO, IMHNPs and PFOB@IMHNPs in aqueous solution at pH 7.4. (e) Normalized maximum absorbance and photographs of aqueous solutions of (i) PFOB@IMHNPs, (ii) PFOB@IHNPs, and (iii) free IR780 at 37 °C over time. (f) Temperature profiles of free IR780 and various IR780-containing NPs in PBS receiving NIR laser irradiation at 808 nm (1.0 W/cm^2) over 5 min.

Table 1
Dynamic light scattering data and drug-loading capacity of NPs.

Sample	Size (D_h, nm)[a]	PDI[a]	DLE (%) (IR780/mTHPC)	DLC (%) (IR780/mTHPC)
HNPs	182.2 ± 2.7	0.15	−/−	−/−
IMNPs	188.4 ± 2.1	0.11	79.4/79.6	7.6/7.8
IMHNPs	186.2 ± 3.9	0.12	74.1/81.3	7.3/7.9
PFOB@HNPs	232.1 ± 6.6	0.23	−/−	−/−
PFOB@IMNPs	253.4 ± 6.1	0.21	78.4/68.5	7.6/6.7
PFOB@IMHNPs	254.2 ± 6.2	0.22	75.1/71.2	7.4/7.0

[a] Determined by DLS measurements.

As shown in the UV/Vis spectra of IMHNPs and PFOB@IMHNPs in aqueous solutions (Fig. 1d), both feature absorption peaks of mTHPC and IR780 were observed at 660 and 780 nm, respectively, indicating the presence of both compounds within NPs. The drug loading data shown in Table 1 also suggest that the effective drug encapsulation is achieved irrespective of the enclosure of PFOB within NPs. It has been recently reported that the practical applications of IR780 in tumor imaging and PTT are limited by its poor photo-stability driven by its rapid self-aggregation and photo-bleaching in aqueous solution [29,30]. As expected, the absorbance of free IR780 species in PBS at 37 °C declined significantly over 4 days as a result of photo-bleaching, in consistence with the color change occurring from the aqueous free IR780 solution as illustrated in the inset of Fig. 1e. In contrast, only a minor reduction in the absorbance was observed for PFOB@IMHNPs and PFOB@IMNPs upon 4-day incubation in PBS. These results demonstrate that encapsulation of IR780 into these lipid-enclosed NPs can remarkably improve its photo-stability in aqueous solution by preventing photo-bleaching reaction. At an IR780 concentration of 20 μM, NIR irradiation at 808 nm induced considerable elevation of the temperature of IR780-carrying NP solutions compared with that of free IR780 solution (Fig. 1f). The NIR-activated photothermal effect of free IR780 is appreciably reduced compared to the IR780-loaded NPs due to the poor aqueous solubility of free IR780. These results support previous findings that have been reported elsewhere [21,29,30]. As observed by Chang's group, the photothermal effect of free IR780 species in aqueous environment was appreciably lower compared to that of PEGylated albumin/IR780/iron oxide nanocomplexes due to its high tendency of forming aggregates in aqueous solution [29].

3.2. *In vitro oxygen delivery and singlet oxygen generation of PFOB droplet NPs*

To evaluate the oxygen delivery of PFOB droplet NPs, the aqueous solutions containing PFOB@HNPs and oxygenated HNPs (as a control) were heated to over 60 °C for 5 min. As the solubility of oxygen in aqueous solutions decreases with increasing temperature, oxygen

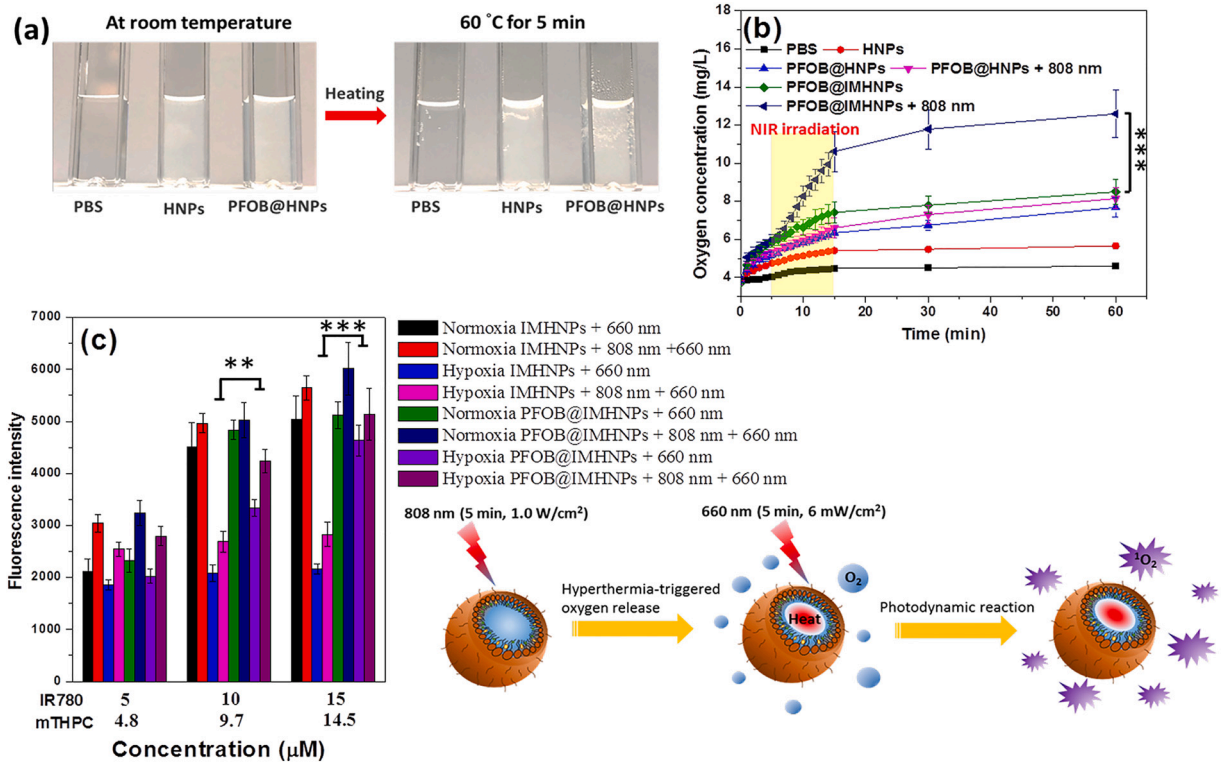

Fig. 2. (a) Photographs of aqueous solutions of HNPs and PFOB@IMHNPs before and after heating. (b) Oxygen release from various NPs with or without irradiation using an 808-nm NIR laser. (c) Fluorescence intensity of oxidized SOSG in aqueous solutions of PFOB@IMHNPs and oxygenated IMHNPs under normoxic and hypoxic conditions with irradiation at 660 nm (5 min, 6 mW/cm^2) alone or 880 nm (5 min, 1.0 W/cm^2) plus 660 nm (5 min, 6 mW/cm^2). The schematic illustration of hyperthermia-triggered oxygen release and photodynamic reaction of PFOB@IMHNPs exposed to sequential NIR irradiation at 808 and 660 nm are also included.

bubbles were generated in the aforementioned solutions, which was particularly obvious in the case of PFOB@HNPs (Fig. 2a). This indicates that PFOB@HNPs can carry more oxygen molecules and promote oxygen liberation in response to increased external temperature. Since PFOB@HNPs exhibited enhanced thermo-responsive oxygen release, it implies that IR780-mediated photothermal conversion of PFOB@IMHNPs can be adopted as a stimulus to trigger oxygen liberation. As shown in Fig. 2b, irradiation at 808 nm for 10 min resulted in a remarkable increase in the oxygen concentration of the PFOB@IMHNP solution compared with that of PBS without any irradiation. This demonstrates the thermo-triggered burst release of oxygen from PFOB@IMHNPs. In contrast, because of the lack of hyperthermia, the oxygen concentrations of the PFOB@HNP solution irradiated with NIR and of PFOB@IMHNP solution without NIR laser irradiation only increased slightly. On the basis of the aforementioned findings, it is very likely that PFOB@IMHNPs could prevent oxygen leakage during blood circulation and selectively release oxygen to reduce tumor hypoxia in response to NIR irradiation once the particles accumulate in tumor sites. Therefore, the efficacy of PDT in particular in tumor hypoxia regions can be highly enhanced by adopting PFOB@IMHNPs as an oxygen self-sufficient NP-based photosensitizer system. To prove the theory, the generation of singlet oxygen species from oxygen-carrying PFOB@IMHNPs in combination with mTHPC-mediated photodynamic reaction under hypoxic conditions was examined using an SOSG assay [5,16]. As illustrated in Fig. 2c, under normoxic conditions with irradiation at 660 nm, oxygenated IMHNP and PFOB@IMHNP solutions exhibited similar fluorescence intensities of oxidized SOSG. This demonstrates that the ROS generation capabilities of IMHNPs and PFOB@IMHNPs through the mTHPC-mediated photodynamic effect are comparable. Notably, in hypoxic conditions with irradiation at 660 nm, the fluorescence intensity of oxidized SOSG in the PFOB@IMHNP solution was remarkably higher than that of oxidized SOSG in the IMHNP solution. Comparatively, singlet oxygen production from PFOB@IMHNPs was robustly maintained under hypoxic conditions, suggesting that the oxygen-carrying capability of PFOB in the core of PFOB@IMHNPs could contribute considerably to the photodynamic effect of encapsulated mTHPC. Furthermore, under normoxic or hypoxic conditions, the fluorescence intensity of oxidized SOSG in PFOB@IMHNP and oxygenated IMHNP solutions that were exposed to sequential irradiation at 808 and 660 nm was somewhat higher than that of oxidized SOSG when irradiation at 660 nm was carried out alone. Several previous studies have shown that IR780 exhibits dual photothermal and photodynamic effects [5,17,31]. Together with the aforementioned results, this implies that hyperthermia-triggered oxygen release and mTHPC/IR780-induced photodynamic reaction promote singlet oxygen production (Fig. 2c).

3.3. *In vitro acid-mediated cellular uptake*

The influence of pH-sensitive surface-charge conversion of PFOB@IMHNPs on cellular uptake of NPs was explored using TRAMP-C1 cells. When the culture was adjusted from pH 7.4 to 6.5, the NIR fluorescence intensity of IR780 in TRAMP-C1 cells incubated with PFOB@IMHNPs was considerably increased compared with that in cancer cells treated with PFOB@IMNPs or IR780/mTHPC mixtures (Fig. 3a). The flow cytometric measurements also illustrate the significant increase of the mTHPC fluorescence intensity in TRAMP-C1 cancer cells treated with PFOB@IMHNPs in response to the pH reduction from 7.4 to 6.5 (Fig. 3b). These findings strongly suggest that, in weakly acidic conditions, the positive surface charge of PFOB@IMHNPs increases because of protonation of imidazole moieties of the NAcHis-TPGS, which then promotes cellular uptake of the NPs by virtue of the increased electrostatic attraction of the positive charges on NP surfaces with negative charges on cell membranes. The CLSM images and quantified mTHPC fluorescence intensity data correlate with the aforementioned results, revealing that the delivery of mTHPC by PFOB@IMHNPs at

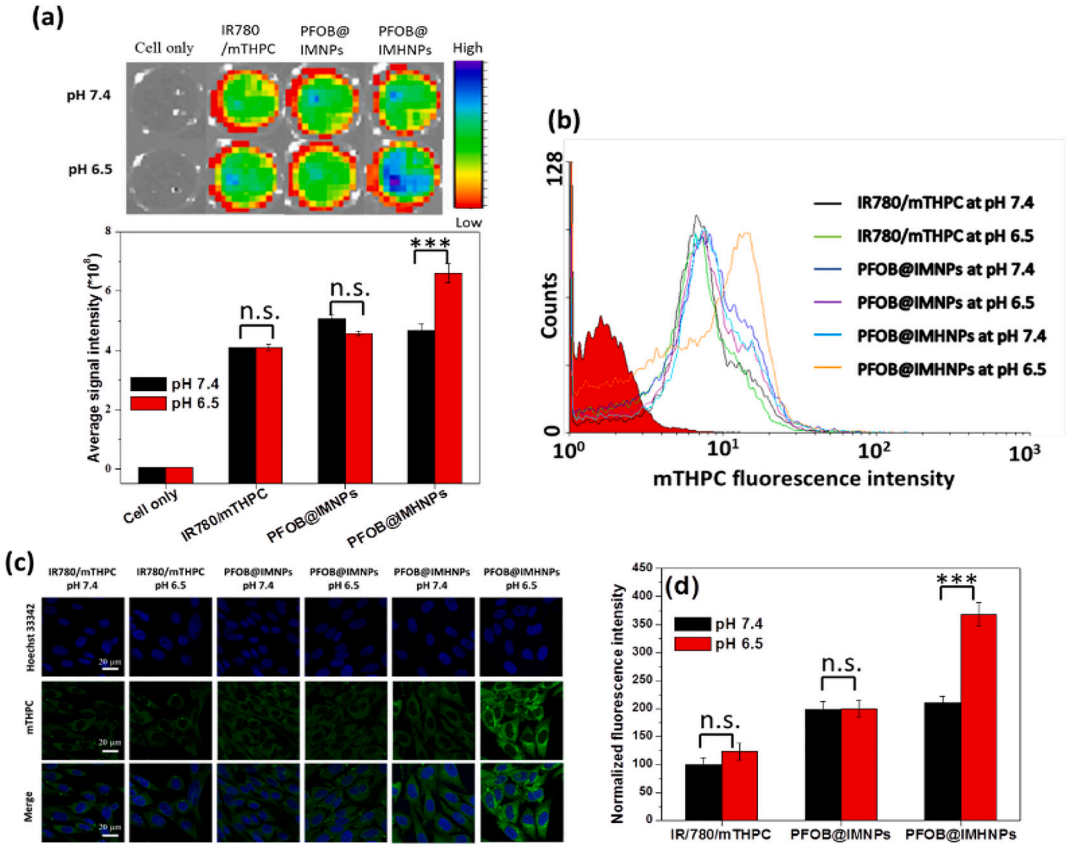

Fig. 3. (a) NIR fluorescence images and intensity of IR780 molecules from TRAMP-C1 cells following incubation with IR780/mTHPC mixtures and various NPs at pH 6.5 or 7.4 by IVIS measurements. (b) Flow cytometric histograms, (c) CLSM images, and (d) quantified mTHPC fluorescence intensity of TRAMP-C1 cells following incubation with IR780/mTHPC mixtures and various NPs at pH 6.5 or 7.4 for 4 h. Cells were stained with Hoechst 33342 to identify cell nuclei. Scale bars are 20 μm. $^{*}P < 0.05$, $^{**}P < 0.01$, $^{***}P < 0.001$.

pH 6.5 into TRAMP-C1 cells is appreciably enhanced as compared to that by PFOB@IMHNPs at pH 7.4 or by PFOB@IMNPs at either pH 7.4 or 6.5 (Fig. 3c and d).

3.4. Intracellular generation of singlet oxygen

The intracellular singlet oxygen production by PFOB@IMHNPs was assessed using a DCFH-DA assay followed by CLSM examination. Fig. 4 illustrates that TRAMP-C1 cells incubated with either PFOB@IMHNPs or IMHNPs at pH 7.4 under normoxic conditions and then subjected to irradiation at 808 and 660 nm exhibited significantly increased DCF fluorescence intensity compared with untreated TRAMP-C1 cells exhibiting only low DCF fluorescence. This confirms that the PFOB@IMHNPs and IMHNPs could effectively generate singlet oxygen through NIR-triggered photodynamic reaction within normoxic cancer cells. Moreover, when TRAMP-C1 cells were incubated with IMHNPs in hypoxic conditions, the intracellular DCF fluorescence intensity did not increase significantly following irradiation, indicating that the singlet oxygen generation within hypoxic cancer cells was rather limited because of the low intracellular oxygen concentrations. Notably, the strong DCF fluorescence within hypoxic TRAMP-C1 cells that were incubated with PFOB@IMHNPs at pH 6.5 and 7.4 following irradiation with dual NIR lasers (808 nm and 660 nm) suggested that PFOB@IMHNPs produced singlet oxygen within hypoxic cells *via* intracellular oxygen delivery combined with the NIR-activated photodynamic effect.

3.5. In vitro efficacy of combined PT/PD therapy of cargo-carrying NPs

The *in vitro* anticancer potency of the cargo-containing NPs in PT/PD combination therapy was evaluated in terms of the viability of TRAMP-C1 cells treated with NP therapeutics following single- and dual-modality treatments under normoxic or hypoxic conditions by MTT assay. Consistent with the results of our previous work [10], TRAMP-C1 cells irradiated without the NP treatment (control group) showed viability of over 95%, indicating that NIR irradiation does not affect the viability of cancer cells. Furthermore, high viability (> 85%) of TRAMP-C1 cells was observed following incubating with various drug-free PFOB droplet NPs, which confirms that these DPPC membrane-enclosed PFOB droplets are not toxic toward TRAMP-C1 cells (Fig. S5). As shown in Fig. 5a, the viability of TRAMP-C1 cells incubated with PFOB@IMHNPs and IMHNPs with the same drug doses under normal oxygen conditions at pH 7.4 or 6.5 was significantly reduced upon irradiation at 808 and 660 nm compared with that of cells that were only irradiated with the 660-nm NIR laser. This shows that the PT/PD combination therapy delivered by either PFOB@IMHNPs or IMHNPs kills cancer cells more effectively in normoxic conditions than PDT alone. Notably, after irradiation with dual NIR lasers, TRAMP-C1 cells incubated with IMHNPs in hypoxic conditions maintained relatively high viability compared with that from the IMHNP treatment in normoxic conditions (Fig. 5a and b). A similar result was attained for TRAMP-C1 cells treated with IMHNPs in either normoxic or hypoxic conditions followed by irradiation at 660 nm alone. These findings indicate that the PDT-related anticancer activity of IMHNPs toward hypoxic cancer cells was reduced as primarily a result of the suppressed singlet oxygen generation because of low intracellular oxygen levels. In contrast, intracellular oxygen delivery caused highly potent anticancer activity of PFOB@IMHNPs toward hypoxic TRAMP-C1 cells through dual NIR-triggered PT/PD combination therapy, as demonstrated by the reduced cell viability shown in Fig. 5b. It should be noted that, when the pH of culture medium was adjusted from 7.4 to 6.5, a decrease in

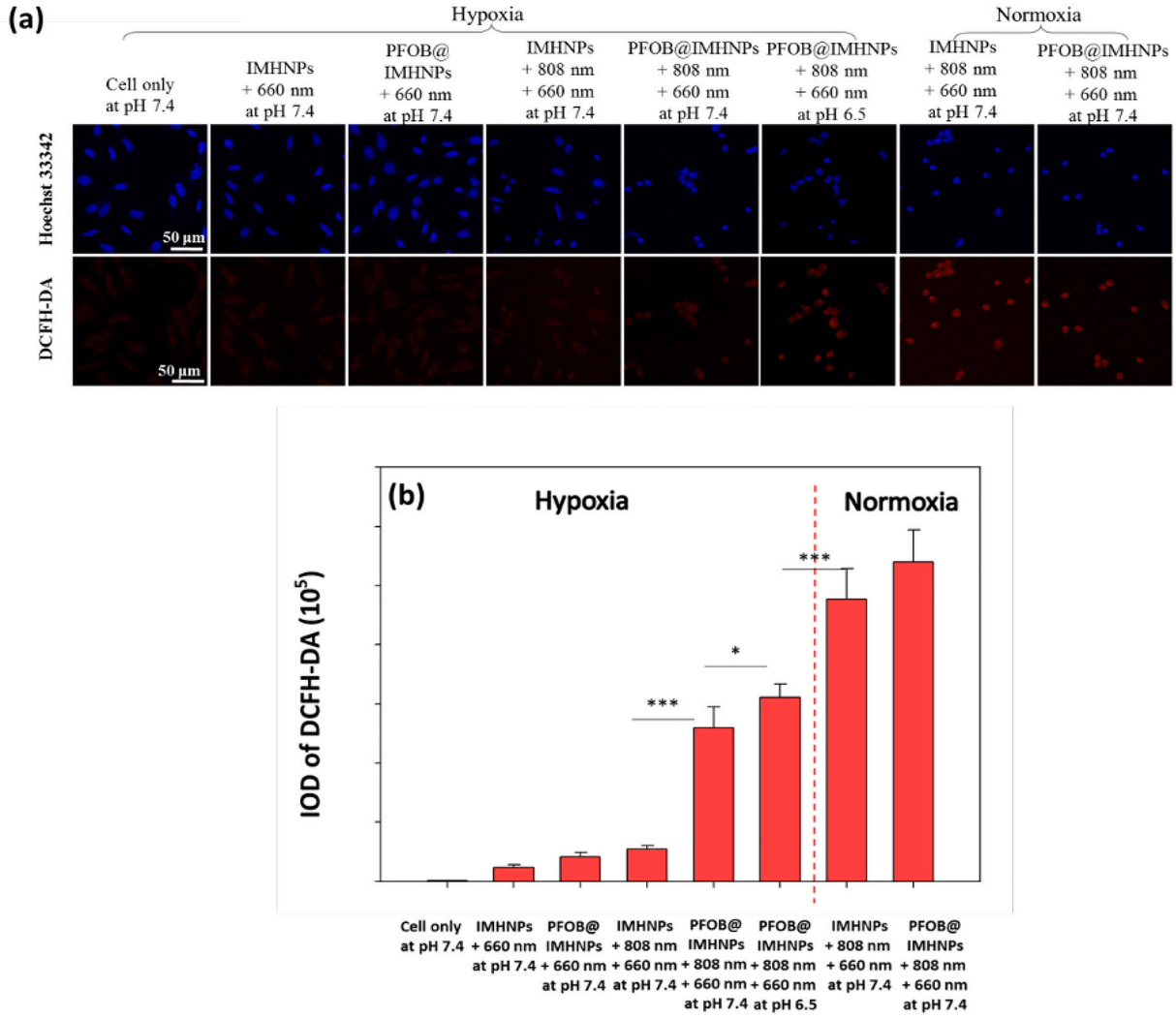

Fig. 4. (a) CLSM images and (b) quantified DCF fluorescence intensity of TRAMP-C1 cells as a measure of intracellular ROS generation following incubation with PFOB@IMHNPs and IMHNPs in normoxic or hypoxic conditions and irradiation at either 660 (5 min, 6 mW/cm^2) or 808 nm (5 min, 1.0 W/cm^2) followed by 660 nm (5 min, 6 mW/cm^2). Cells were stained with Hoechst 33342 to visualize cell nuclei. Scale bars are 50 μm. *$P < 0.05$, **$P < 0.01$, ***$P < 0.001$.

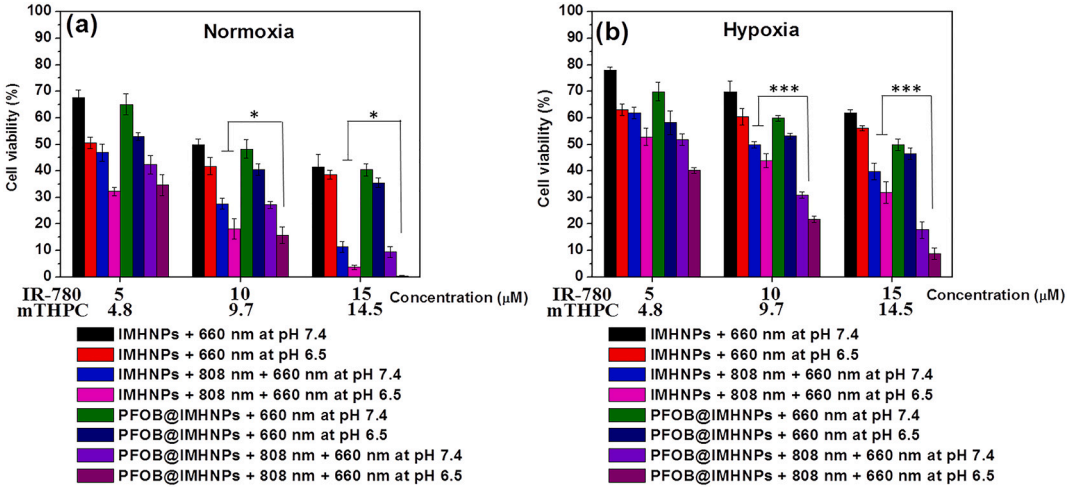

Fig. 5. Cell viability of TRAMP-C1 cells treated with PFOB@IMHNPs and IMHNPs under normoxic or hypoxic conditions followed by irradiation at either 660 (5 min, 6 mW/cm^2) or 808 nm (5 min, 1.0 W/cm^2) followed by 660 nm (5 min, 6 mW/cm^2). *$P < 0.05$, **$P < 0.01$, ***$P < 0.001$.

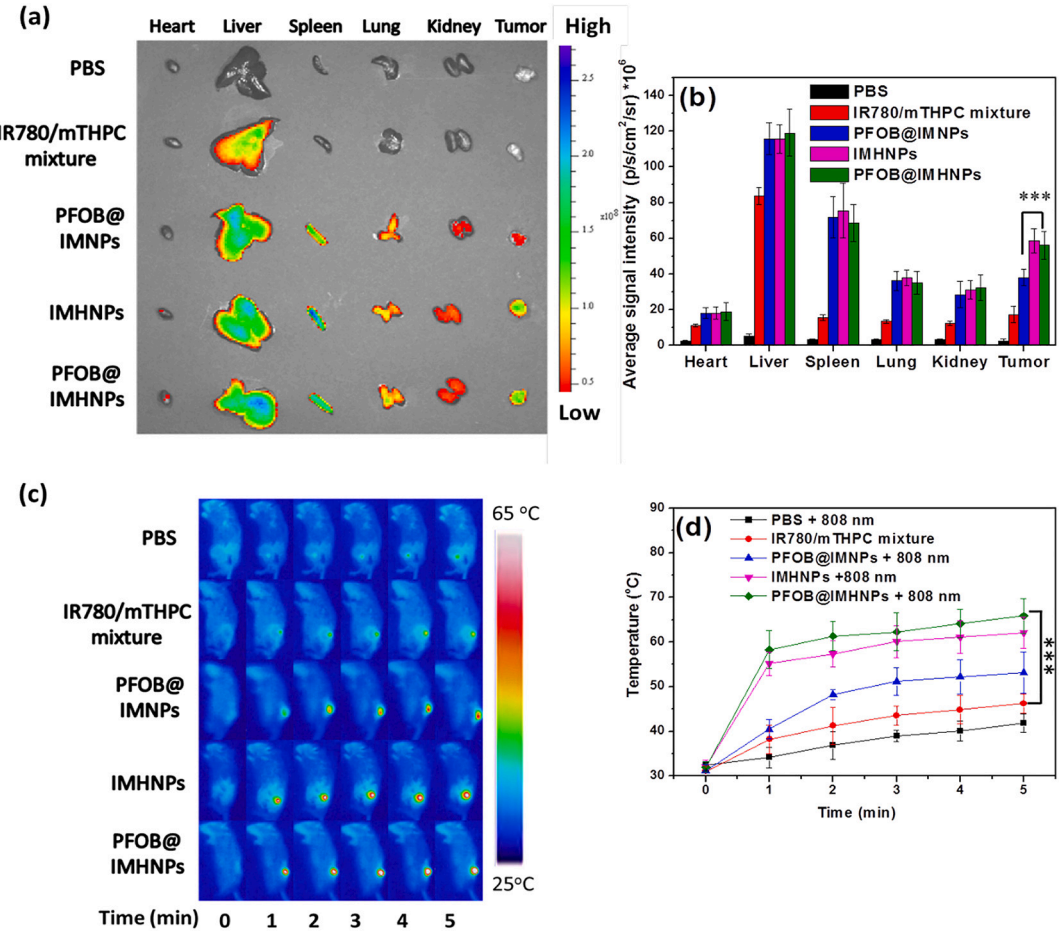

Fig. 6. (a) IVIS fluorescence images and (b) average IR780 fluorescence intensities of isolated tumors and major organs at 24 h after injection with PBS or various IR780-containing formulations. (c) IR thermographic maps and (d) temperature profiles of the tumor regions of TRAMP-C1 tumor-bearing mice treated with various formulations followed by irradiation at 808 nm (5 min, 1.0 W/cm^2). $^*P < 0.05$, $^{**}P < 0.01$, $^{***}P < 0.001$.

cell viability of TRAMP-C1 cells treated with combined PTT and PDT delivered by PFOB@IMHNPs and IMHNPs under normoxic or hypoxic conditions. This suggests that the acid-activated cellular internalization of these NPs amplifies the anticancer effects of PTT and PDT.

3.6. *In vivo* biodistribution of NPs and NIR-triggered tumor hyperthermia

The effects of the acid-triggered surface-charge conversion of PFOB@IMHNPs on *in vivo* tumor accumulation and biodistribution were investigated using the TRAMP-C1 tumor model in male C57BL/6 J mice. PFOB@IMNPs, IMHNPs, and free mTHPC/IR780 mixtures were adopted as control groups. The IVIS examination on major organs and tumor samples (Fig. 6a and b) revealed no detectable *ex vivo* NIR fluorescence signals of IR780 in tumor samples following free mTHPC/IR780 administration by intravenous injection, whereas higher fluorescence signals of IR780 were detected within tumor samples following administration of PFOB@IMHNPs, PFOB@IMNPs, or IMHNPs, most obviously in the cases of PFOB@IMHNPs and IMHNPs. This suggests that these cargo-loaded NPs are retained at the tumor, likely through the enhanced permeability and retention effects. In contrast, free IR780 showed poor tumor accumulation due to the rapid removal from the body resulting from IR780 aggregation in blood circulation. Furthermore, tumor accumulation of PFOB@IMHNPs and IMHNPs was further enhanced compared with PFOB@IMNPs. It is ascribed to the increased cellular uptake due to the increased NP surface positive charges in response to the tumor acidic extracellular environment. In contrast, the *ex vivo* NIR fluorescence signals of livers of tumor-bearing mice treated with IR780-containing NPs were considerably higher compared with those of other organs due to inevitable NP uptake by the reticuloendothelial system. Similar biodistributions of NP-based drug-delivery systems have been observed in tumor-bearing mice in other studies [32–34]. In view of the favorable biocompatibility and biodegradability of DPPC, cholesterol, NAcHis-TPGS and PFOB used as the main components of cargo-loaded NPs, it is expected that the cargo-carrying NPs accumulated in liver be gradually degraded and eliminated from body.

The NIR-triggered *in vivo* tumor hyperthermia of tumor-bearing mice injected intravenously with IR780-containing nanoformulations was monitored by infrared thermal imaging. Upon irradiation at 808 nm 24 h after intravenous injection, administration of PFOB@IMHNP and IMHNP caused significantly enhanced local tumor temperatures compared with free mTHPC/IR780 mixture or PFOB@IMNPs, due to the increased tumor uptake and tumor accumulation of IR780 (Fig. 6a and d). Notably, after 5-min irradiation with the 808-nm NIR laser, tumor temperatures of the PFOB@IMHNP and IMHNP groups were above 55 °C. Such NIR-activated tumor hyperthermia could result in irreversible heat ablation against cancer cells.

3.7. *In vivo* tumor-targeted oxygen delivery

In order to evaluate the tumor hypoxia-targeted oxygen delivery ability of PFOB@IMHNPs pre-saturated with oxygen, tumor hypoxia status was analyzed by IHC staining of tumor sections. As shown in Fig. 7a and S6a, the tumors receiving either PFOB@IMHNPs or IMHPNs without NIR laser irradiation of 808 nm showed similar mTHPC fluorescence intensity, being indicative of the comparable tumor

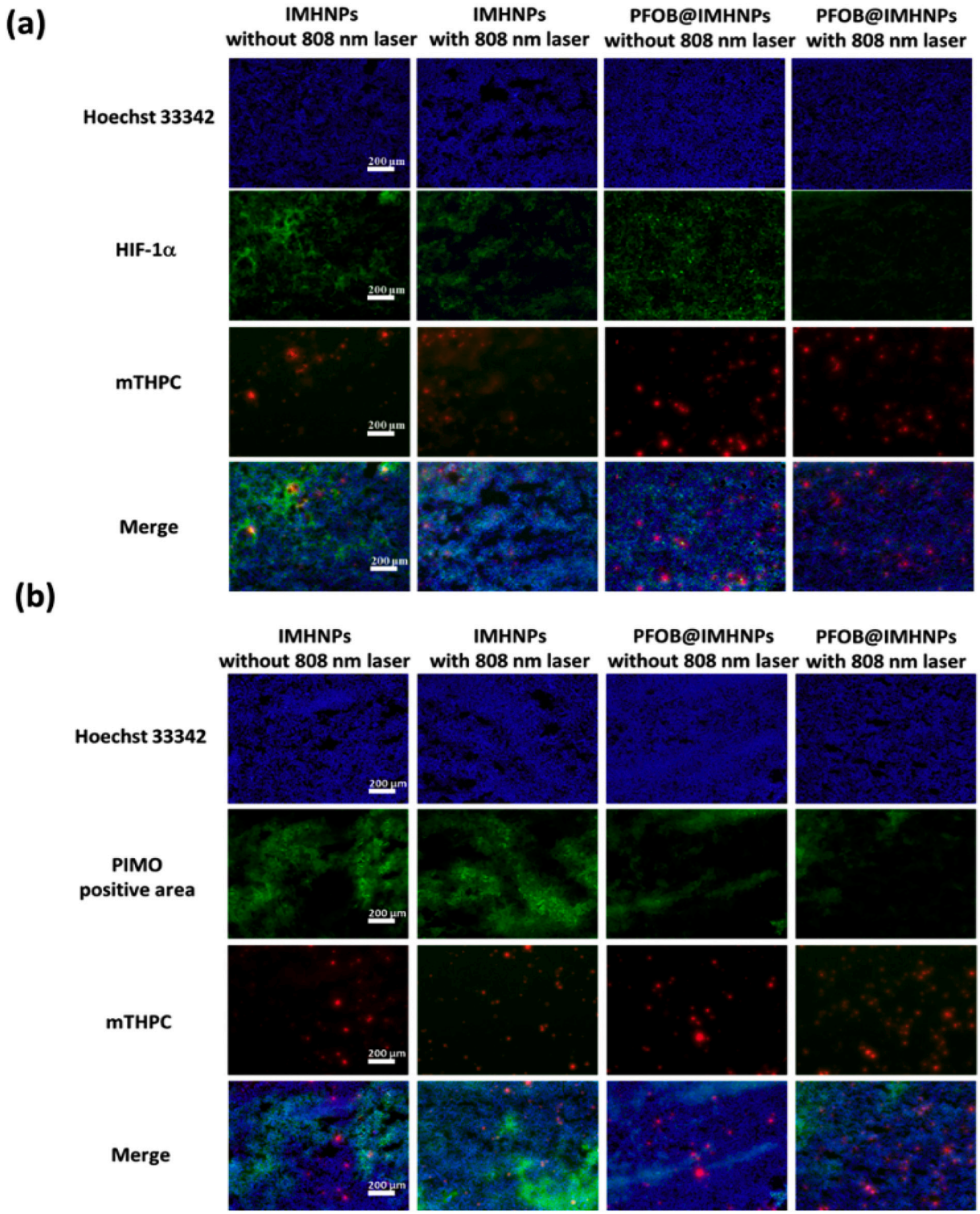

Fig. 7. Fluorescence images of tumor sections from TRAMP-C1 tumor-bearing mice receiving the NP therapeutics with or without NIR laser irradiation at 808 nm. Tumor cell nuclei were stained with Hoechst in blue, and tumor hypoxia was stained with (a) HIF-1α and (b) PIMO markers (in green), respectively. Scale bars are 200 μm. (For interpretation of the references to color in this figure legend, the reader is referred to the web version of this article.)

accumulation of mTHPC delivered by the NPs. Importantly, tumors treated with PFOB@IMHNPs and irradiation at 808 nm in sequence exhibited reduced fluorescence of HIF-1α marker as a measure of tumor hypoxia (Fig. 7a). Similarly, tumors receiving PFOB@IMHNPs and irradiation at 808 nm exhibited considerably decreased fluorescence of PIMO marker (Fig. 7b and S6b), suggesting that accumulation of PFOB@IMHNPs within the tumor caused a remarkable increase in oxygen release through NIR-triggered hyperthermia, thus relieving tumor hypoxia. In contrast, the fluorescence intensity of HIF-1α and PIMO markers in tumors treated with IMHNPs and irradiated at 808 nm remained strong, confirming that IMHNPs did not reduce tumor hypoxia due to a lack of oxygen-carrying ability. On the basis of these findings, it can be concluded that PFOB@IMHNPs are an effective antitumor agent for NIR-triggered PTT and enhance the effects of PDT *via*

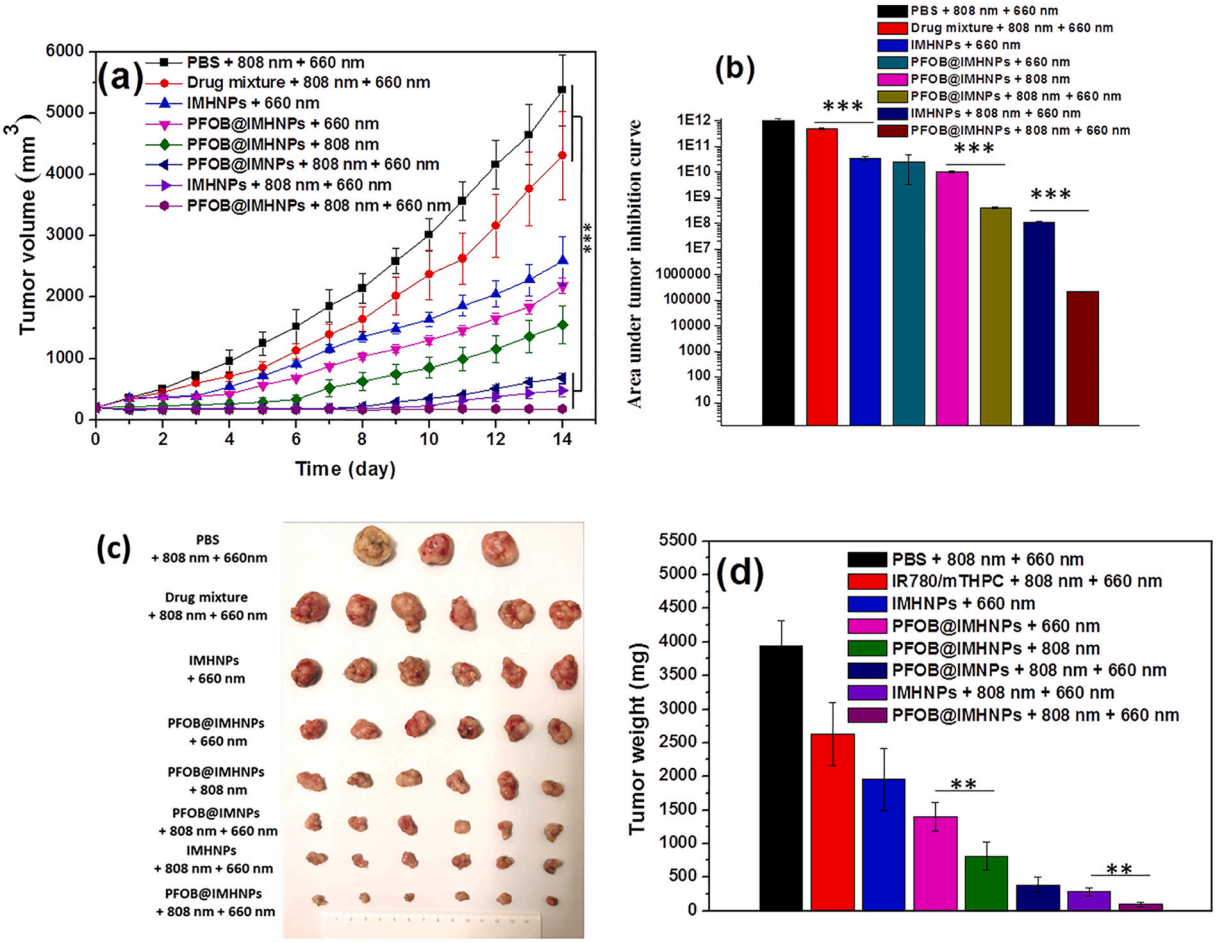

Fig. 8. (a) Tumor growth profiles and (b) area under the curve of tumor growth from TRAMP-C1 tumor-bearing mice treated with different formulations by intravenous injection followed by NIR irradiation at 24 h post-injection ($n = 6$ per group). (c) Photo-image and (d) mass of tumors isolated from sacrificed mice. $^{*}P < 0.05$, $^{**}P < 0.01$, $^{***}P < 0.001$.

tumor-targeted oxygen delivery.

3.8. Inhibition of in vivo tumor growth by combined PT/PD therapy

To evaluate the *in vivo* antitumor efficacy of the functionalized NP therapeutics in oil droplet structure, tumor sizes were monitored in TRAMP-C1 tumor-bearing mice following intravenous injection with various drug-containing formulations and subsequent NIR laser irradiation. As shown in Fig. S7, no significant variations were observed in the body weights of any treated mice. This demonstrates that the formulations used did not cause serious acute toxicity. Notably, 14 days after intravenous injection and irradiation with dual NIR lasers, the tumor volumes of mice receiving free mTHPC/IR780 treatment were increased significantly with time in a similar manner to that of the PBS group (Fig. 8a). Free mTHPC/IR780 treatment obviously failed to suppress tumor growth, primarily due to the poor tumor uptake of free IR780 as aforementioned (Fig. 6a and b) as well as the strong tendency of hydrophobic mTHPC to form aggregates in biological fluids that reduce singlet oxygen production [35,36]. Moreover, during the initial 8 days of treatment, PTT/PDT combination therapy delivered by PFOB@IMHNPs, PFOB@IMNPs, or IMHNPs resulted in sound inhibition in tumor growth compared with single PDT or PTT. Compared to the nanostructured porphyrin assembly developed by Zheng's group that effectively suppressed the growth of hypoxic tumor *in vivo* by single PTT [37], the IR780-loaded nanoparticles developed in this work were found incapable of fully inhibiting tumor growth based on sole PTT. This is attributed to that the tumor volume (ca 200 mm^3) at the onset of therapy in this study is significantly larger than that (ca 30 mm^3) adopted in Zheng's work. In general, a relatively small tumor could be completely eradicated by PTT, while a large tumor receiving single-dose PTT is apt to recur due to the proliferation of residual cells within deep tumor hypoxic region. In this regard, in order to improve the antitumor efficacy by killing remaining cancer cells in heterogeneous tumor hypoxia with PDT, it is necessary to achieve the tumor-targeted delivery of the combination therapy and supplementary oxygen.

After that, it was found that the tumors gradually enlarged in size with time over 14 days for the PFOB@IMNPs and IMHNPs groups receiving the PT/PD combination therapy (Fig. 8a). In contrast, the tumors remained essentially the same size with the combination therapy in the PFOB@IMHNPs group (Fig. 8a and S8), manifesting the full inhibition of tumor growth in this group. Individual time-evolved tumor growth profiles of treated mice with dual phototherapies, respectively, from PFOB@IMHNPs, PFOB@IMNPs and IMHNPs are illustrated in Fig. S8. Furthermore, the quantified data from the areas under the curve of tumor growth (Fig. 8b) also demonstrate the best therapeutic effect of the combined PTT/PDT treatment from the PFOB@IMHNPs group. Consistent with the suppression of *in vivo* tumor growth, tumors that were harvested from mice treated with combined PT/PD therapy from PFOB@IMHNPs were smallest in size and lowest in weight (Fig. 8c and d). Because of the outstanding performance of PFOB@IMHNPs in tumor-targeted delivery of drugs and oxygen, it is concluded that NIR-triggered PT/PD combination therapy alongside self-sufficient oxygen delivery can effectively kill cancer cells in hypoxic and normoxic

regions of tumors, thus fully inhibiting tumor growth. Although the promising *in vivo* results were obtained in this study, there are still several challenges for the clinical applications of cancer phototherapy. Certainly, for several types of cancers, such as oral cancer and skin cancers, selective light irradiation at tumor sites can be realized with the help of optical fibers, thus attaining satisfied therapeutic outcome [38]. Unfortunately, the therapeutic efficacy of PTT and PDT was compromised for some other deeply located cancers. In order to improve the performance of phototherapeutic nanomedicine, the development of easy-to-use medical equipment that can deliver light into deep tissues is thus essentially required

4. Conclusions

In this study, a tumor mild acidity-responsive PFOB droplet NPs was successfully developed, which shows excellent capability of carrying oxygen, IR780, and mTHPC for enhancing the antitumor potency of PTT/PDT combination therapy *via* promotion of the tumor-targeted delivery of photosensitizers and oxygen molecules. Through self-sufficient oxygen supplementation and acid-activated cellular uptake, the tailor-made NPs (PFOB@IMHNPs) effectively facilitated intracellular delivery of IR780 and mTHPC and produced singlet oxygen within hypoxic TRAMP-C1 cells through NIR-triggered photothermal/photodynamic effects, thereby exhibiting pronounced anticancer efficacy *in vitro*. Sequential irradiation at 808 nm then at 660 nm of TRAMP-C1 tumors from tumor-bearing mice receiving PFOB@IMHNPs for the PTT/PDT combination therapy caused full inhibition of tumor growth due to the superior tumor-targeted cargo delivery and relief of tumor hypoxia provided by these functionalized NPs. Both the *in vitro* and *in vivo* results strongly demonstrate great promise of PFOB@IMHNPs as a smart NP therapeutics for effective cancer treatment.

Declaration of Competing Interest

The authors declare no competing financial interests.

Acknowledgments

This work is supported by the Ministry of Science and Technology, Taiwan (MOST 107-2221-E-007-032-MY3 and 108-2314-B-007-004-MY3), National Tsing Hua University, Taiwan (109Q2520E1) and Hsinchu Mackay Memorial Hospital, Taiwan (MMH-TH-10905).

Appendix A. Supplementary data

Supplementary data to this article can be found online at https://doi.org/10.1016/j.jconrel.2020.08.038.

References

[1] L. Cheng, C. Wang, L. Feng, K. Yang, Z. Liu, Functional nanomaterials for phototherapies of cancer, Chem. Rev. 114 (2014) 10869–10939.
[2] M.K. Gnanasammandhan, N.M. Idris, A. Bansal, K. Huang, Y. Zhang, Near-IR photoactivation using mesoporous silica-coated NaYF4:Yb, Er/tm upconversion nanoparticles, Nat. Protoc. 11 (2016) 688–713.
[3] M. Karimi, P. Sahandi Zangabad, S. Baghaee-Ravari, M. Ghazadeh, H. Mirshekari, M.R. Hamblin, Smart nanostructures for cargo delivery: uncaging and activating by light, J. Am. Chem. Soc. 139 (2017) 4584–4610.
[4] K.F. Chu, D.E. Dupuy, Thermal ablation of tumours: biological mechanisms and advances in therapy, Nat. Rev. Cancer 14 (2014) 199–208.
[5] L. Zhang, D. Wang, K. Yang, D. Sheng, B. Tan, Z. Wang, H. Ran, H. Yi, Y. Zhong, H. Lin, Y. Chen, Mitochondria-targeted artificial "Nano-RBCs" for amplified synergistic cancer phototherapy by a single NIR irradiation, Adv. Sci. 5 (2018) 1800049.
[6] W. Li, J. Yang, L. Luo, M. Jiang, B. Qin, H. Yin, C. Zhu, X. Yuan, J. Zhang, Z. Luo, Y. Du, Q. Li, Y. Lou, Y. Qiu, J. You, Targeting photodynamic and photothermal therapy to the endoplasmic reticulum enhances immunogenic cancer cell death, Nat. Commun. 10 (2019) 3349–3365.
[7] B. Du, W. Zhang, C.H. Tung, Layer-by-layer construction of an oxygen generating photo-responsive nanomedicine for enhanced photothermal and photodynamic combination therapy, Chem. Commun. 55 (2019) 5926–5929.
[8] H. Zhu, P. Cheng, P. Chen, K. Pu, Recent progress in the development of near-infrared organic photothermal and photodynamic nanotherapeutics, Biomater. Sci. 6 (2018) 746–765.
[9] Q. Cheng, Z.H. Li, Y.X. Sun, X.Z. Zhang, Controlled synthesis of a core-shell nanohybrid for effective multimodal image-guided combined photothermal/photodynamic therapy of tumors, NPG Asia Mater. 11 (2019) 63–77.
[10] C.C. Hung, W.C. Huang, Y.W. Lin, T.W. Yu, H.H. Chen, S.C. Lin, W.H. Chiang, H.C. Chiu, Active tumor permeation and uptake of surface charge-switchable theranostic nanoparticles for imaging-guided photothermal/chemo combinatorial therapy, Theranostics 6 (2016) 302–317.
[11] F. Yan, W. Duan, Y. Li, H. Wu, Y. Zhou, M. Pan, H. Liu, X. Liu, H. Zheng, NIR-laser-controlled drug release from DOX/IR-780-loaded temperature-sensitive-liposomes for chemo-photothermal synergistic tumor therapy, Theranostics 6 (2016) 2337–2351.
[12] D. Trachootham, J. Alexandre, P. Huang, Targeting cancer cells by ROS-mediated mechanisms: a radical therapeutic approach? Nat. Rev. Drug Discov. 8 (2009) 579–591.
[13] Z. Huang, H. Xu, A.D. Meyers, A.I. Musani, L. Wang, R. Tagg, A.B. Barqawi, Y.K. Chen, Photodynamic therapy for treatment of solid tumors-potential and technical challenges, Technol. Cancer Res. Treat 7 (2008) 309–320.
[14] K. Han, W. Zhang, J. Zhang, Q. Lei, S. Wang, J. Liu, X. Zhang, H. Han, H, acidity-triggered tumor-targeted chimeric peptide for enhanced intra-nuclear photodynamic therapy, Adv. Funct. Mater. 26 (2016) 4351–4361.
[15] Z. Luo, H. Tian, L. Liu, Z. Chen, R. Liang, Z. Chen, Z. Wu, A. Ma, M. Zheng, L. Cai, Tumor-targeted hybrid protein oxygen carrier to simultaneously enhance hypoxia-dampened chemotherapy and photodynamic therapy at a single dose, Theranostics 8 (2018) 3584–3596.
[16] F. Xu, H. Li, Q. Yao, H. Ge, J. Fan, W. Sun, J. Wang, X. Peng, Hypoxia-activated NIR photosensitizer anchoring in the mitochondria for photodynamic therapy, Chem. Sci. 10 (2019) 10586–10594.
[17] W.C. Huang, M.Y. Shen, H.H. Chen, S.C. Lin, W.H. Chiang, P.H. Wu, C.W. Chang, C.S. Chiang, H.C. Chiu, Monocytic delivery of therapeutic oxygen bubbles for dual-modality treatment of tumor hypoxia, J. Control. Release 220 (2015) 738–750.
[18] C. Zhao, H. Deng, J. Xu, S. Li, L. Zhong, L. Shao, Y. Wu, X.J. Liang, "Sheddable" PEG-lipid to balance the contradiction of PEGylation between long circulation and poor uptake, Nanoscale 8 (2016) 10832–10842.
[19] W.C. Huang, S.H. Chen, W.H. Chiang, C.W. Huang, C.L. Lo, C.S. Chern, H.C. Chiu, Tumor microenvironment-responsive nanoparticle delivery of chemotherapy for enhanced selective cellular uptake and transportation within tumor, Biomacromolecules 17 (2016) 3883–3892.
[20] H. Li, Y. Chen, Z. Li, X. Li, Q. Jin, J. Ji, Hemoglobin as a smart pH-sensitive nanocarrier to achieve aggregation enhanced tumor retention, Biomacromolecules 19 (2018) 2007–2013.
[21] I.L. Lu, T.I. Liu, H.C. Lin, S.H. Chang, C.L. Lo, W.H. Chiang, H.C. Chiu, R780-loaded zwitterionic polymeric nanorparticles with acidity-induced agglomeration for enhanced tumor retention, Eur. Polym. J. 122 (2020) 109400.
[22] Z. Yang, N. Sun, R. Cheng, C. Zhao, Z. Liu, X. Li, J. Liu, Z. Tian, pH-multistage responsive micellar system with charge-switch and PEG layer detachment for co-delivery of paclitaxel and curcumin to synergistically eliminate breast cancer stem cells, Biomaterials 147 (2017) 53–67.
[23] T.I. Liu, T.Y. Lu, S.H. Chang, M.Y. Shen, H.C. Chiu*, Dual stimuli-guided lipid-based delivery system of cancer combination therapy, J. Control. Release 318 (2020) 16–24.
[24] E.C. Dreaden, S.W. Morton, K.E. Shopsowitz, J.H. Choi, Z.J. Deng, N.J. Cho, P.T. Hammond, Bimodal tumor-targeting from microenvironment responsive hyaluronan layer-by-layer (LbL) nanoparticles, ACS Nano 8 (2014) 8374–8382.
[25] L. Zhong, L. Xu, Y. Liu, Q. Li, D. Zhao, Z. Li, H. Zhang, H. Zhang, Q. Kan, Y. Wang, J. Sun, Z. He, Transformative hyaluronic acid-based active targeting supramolecular nanoplatform improves long circulation and enhances cellular uptake in cancer therapy, Acta Pharm. Sin. B 9 (2019) 397–409.
[26] M.O. Durymanov, A.A. Rosenkranz, A.S. Sobolev, Current approaches for improving intratumoral accumulation and distribution of nanomedicines, Theranostics 5 (2015) 1007–1020.
[27] C. Grapentin, S. Barnert, R. Schubert, Monitoring the stability of perfluorocarbon nanoemulsions by cryo-TEM image analysis and dynamic light scattering, PLoS One 10 (2015) e.0130674.
[28] Y. Hu, Y. Wang, J. Jiang, B. Han, S. Zhang, K. Li, S.X. Ge, Y. Liu, Preparation and characterization of novel perfluorooctyl bromide nanoparticle as ultrasound contrast agent via layer-by-layer self-assembly for folate-receptor-mediated tumor imaging, Biomed. Res. Int. 2016 (2016) 6381464.
[29] S.Y. Lin, R.Y. Huang, W.C. Liao, C.C. Chuang, C.W. Chang, Multifunctional PEGylated albumin/IR780/iron oxide nanocomplexes for cancer photothermal therapy and MR imaging, Nanotheranostics 2 (2018) 106–116.
[30] K. Wang, Y. Zhang, J. Wang, A. Yuan, M. Sun, J. Wu, Y. Hu, Self-assembled IR780-loaded transferrin nanoparticles as an imaging, targeting and PDT/PTT agent for cancer therapy, Sci. Rep. 6 (2016) 27421.
[31] G. Yang, J. Tian, C. Chen, D. Jiang, Y. Xue, C. Wang, Y. Gao, W. Zhang, An oxygen self-sufficient NIR-responsive nanosystem for enhanced PDT and chemotherapy against hypoxic tumors, Chem. Sci. 10 (2019) 5766–5772.
[32] Y.C. Tsai, P. Vijayaraghavan, W.H. Chiang, H.H. Chen, T.I. Liu, M.Y. Shen, A. Omoto, M. Kamimura, K. Soga, H.C. Chiu, Targeted delivery of functionalized upconversion nanoparticles for externally triggered photothermal/photodynamic therapies of brain glioblastoma, Theranostics 8 (2018) 1435–1448.
[33] X. Zhang, R. Zhang, J. Huang, M. Luo, X. Chen, Y. Kang, J. Wu, Albumin enhances PTX delivery ability of dextran NPs and therapeutic efficacy of PTX for colorectal

cancer, J. Mater. Chem. B 7 (2019) 3537–3545.
[34] J. Yang, W. Li, L. Luo, M. Jiang, C. Zhu, B. Qin, H. Yin, X. Yuan, X. Yin, J. Zhang, Z. Luo, Y. Du, J. You, Hypoxic tumor therapy by hemoglobin-mediated drug delivery and reversal of hypoxia-induced chemoresistance, Biomaterials 182 (2018) 145–156.
[35] M. Triesscheijn, M. Ruevekamp, R. Out, T.J. Van Berkel, J. Schellens, P. Baas, F.A. Stewart, The pharmacokinetic behavior of the photosensitizer meso-tetra-hydroxyphenyl-chlorin in mice and men, Cancer Chemother. Pharmacol. 60 (2007) 113–122.
[36] Y. Liu, L. Scrivano, J.D. Peterson, M.H.A.M. Fens, I.B. Hernández, B. Mesquita, J.S. Toraño, W.E. Hennink, C.F. van Nostrum, S. Oliveira, EGFR-targeted nanobody functionalized polymeric micelles loaded with mTHPC for selective photodynamic therapy, Mol. Pharm. 17 (2020) 1276–1292.
[37] C.S. Jin, J.F. Lovell, J. Chen, G. Zheng, Ablation of hypoxic tumors with dose-equivalent photothermal, but not photodynamic, therapy using a nanostructured porphyrin assembly, ACS Nano 7 (2013) 2541–2550.
[38] D. Gao, X. Guo, X. Zhang, S. Chen, Y. Wang, T. Chen, G. Huang, Y. Gao, Z. Tian, Z. Yang, Multifunctional phototheranostic nanomedicine for cancer imaging and treatment, Mater. Today Bio 5 (2020) 100035.